Supplemental Information

Article

Material Discovery and High Throughput Exploration of Ru Based Catalysts for Low Temperature Ammonia Decomposition

Katherine McCullough, Pei-Hua Chiang, Juan D. Jimenez, and Jochen A. Lauterbach *

Department of Chemical Engineering University of South Carolina, Columbia, SC 29208, USA; mccullke@email.sc.edu (K.M.); pchiang@email.sc.edu (P.C.); jiminezj@email.sc.edu (J.D.J.)

* Correspondence: lauteraj@cec.sc.edu

Received: 21 February 2020; Accepted: 14 April 2020; Published: date

Thermodynamic Limit

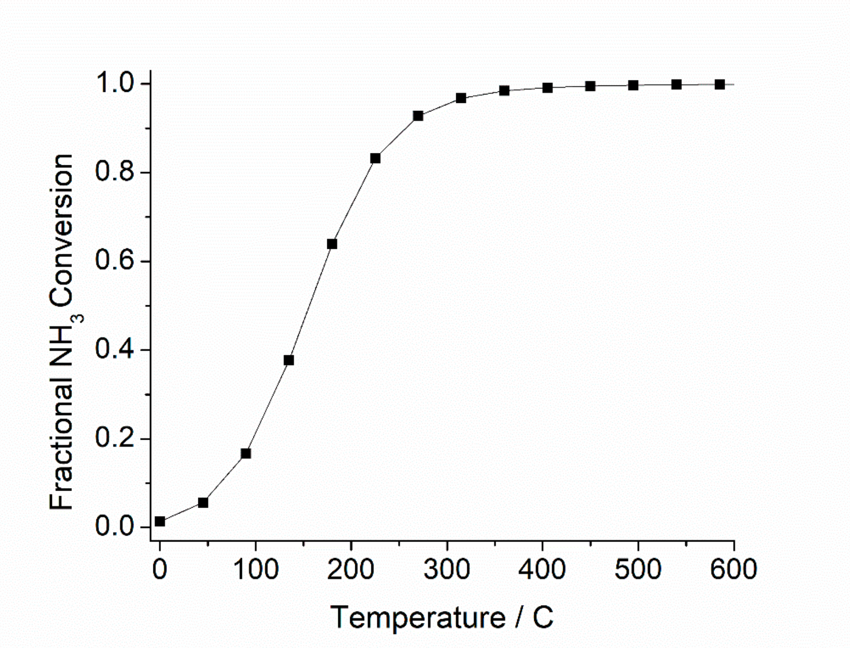

Figure S1. Thermodynamic limit of ammonia decomposition at 101.325 kPa total pressure.

High throughput screening results

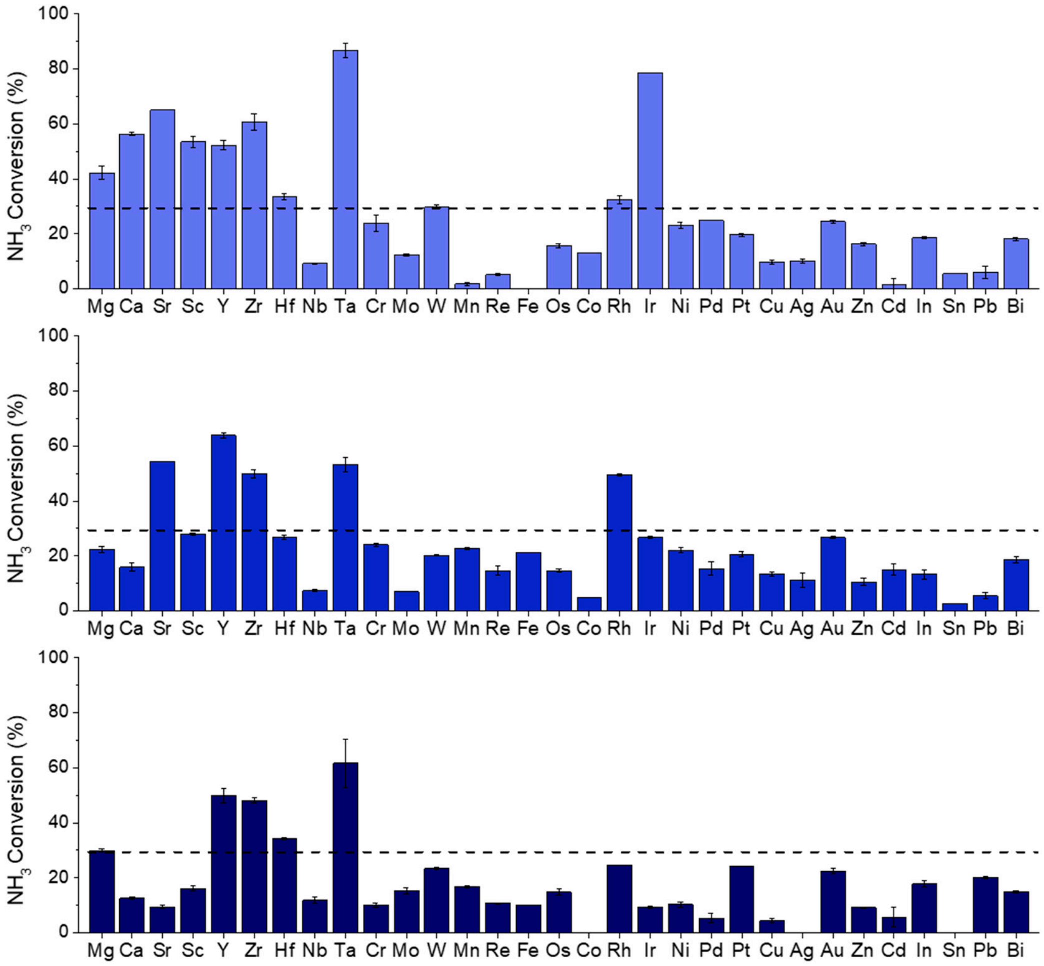

Figure S2. Catalytic activity at 250°C. From bottom to top: 3,1,12 RuMK, 2,2,12 RuMK, and 1,3,12 RuMK, where M is the substituted metal, denoted in the x axis. The black dashed line indicates the activity of the baseline 4,12 RuK catalyst at 250°C. Reaction conditions: 1% NH3 in balance Ar, 30,000 mL/hr/gcat, 1 bar.

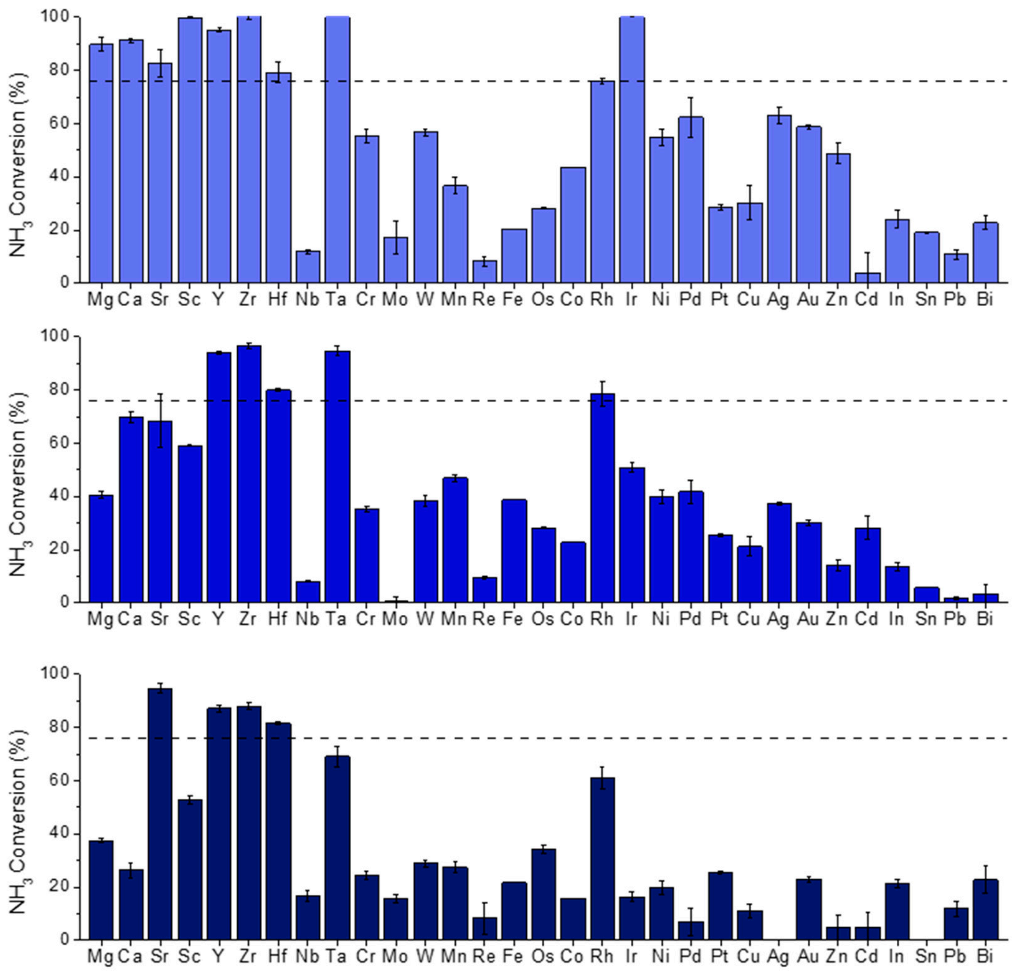

Figure S3. Catalytic activity at 350°C. From bottom to top: 3,1,12 RuMK, 2,2,12 RuMK, and 1,3,12 RuMK, where M is the substituted metal, denoted in the x axis. The black dashed line indicates the activity of the baseline 4,12 RuK catalyst at 350°C. Reaction conditions: 1% NH3 in balance Ar, 30,000 mL/hr/gcat, 1 bar.

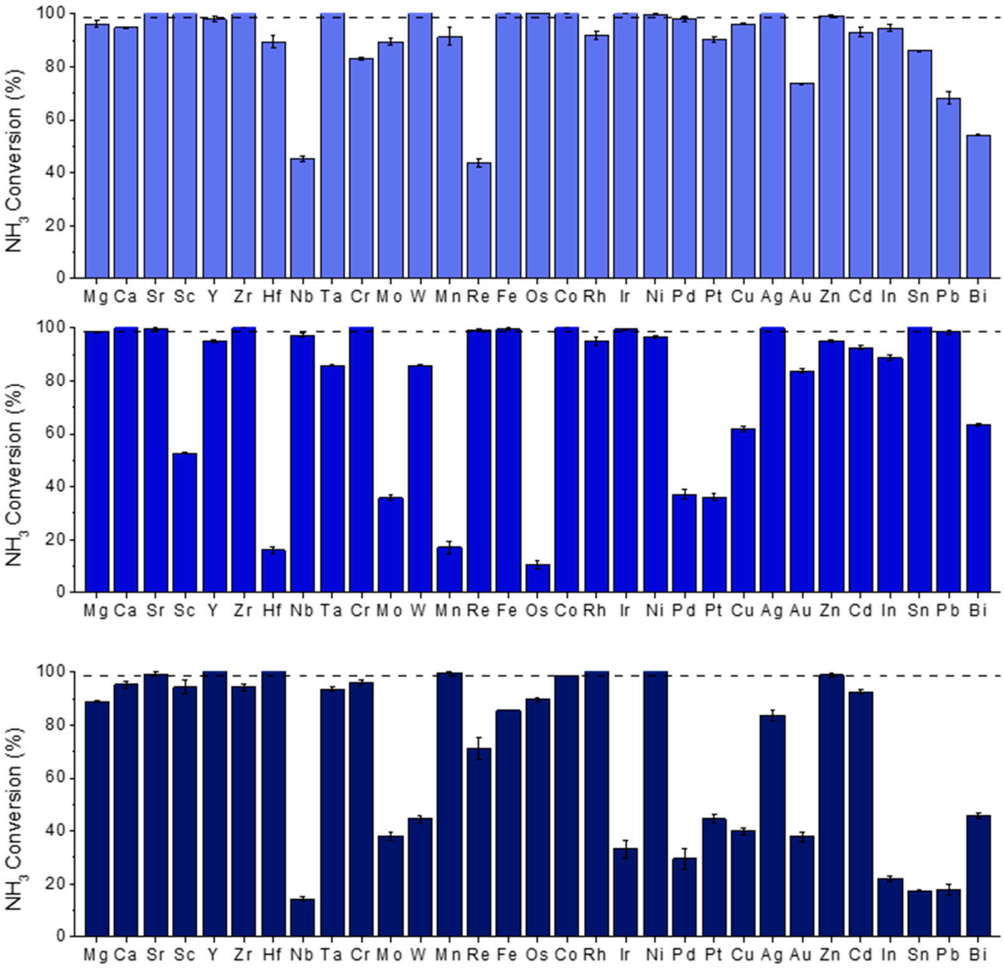

Figure S4. Catalytic activity at 400°C. From bottom to top: 3,1,12 RuMK, 2,2,12 RuMK, and 1,3,12 RuMK, where M is the substituted metal, denoted in the x axis. The black dashed line indicates the activity of the baseline 4,12 RuK catalyst at 400°C. Reaction conditions: 1% NH3 in balance Ar, 30,000 mL/hr/gcat, 1 bar.

Evaluation of Apparent Activation Energy

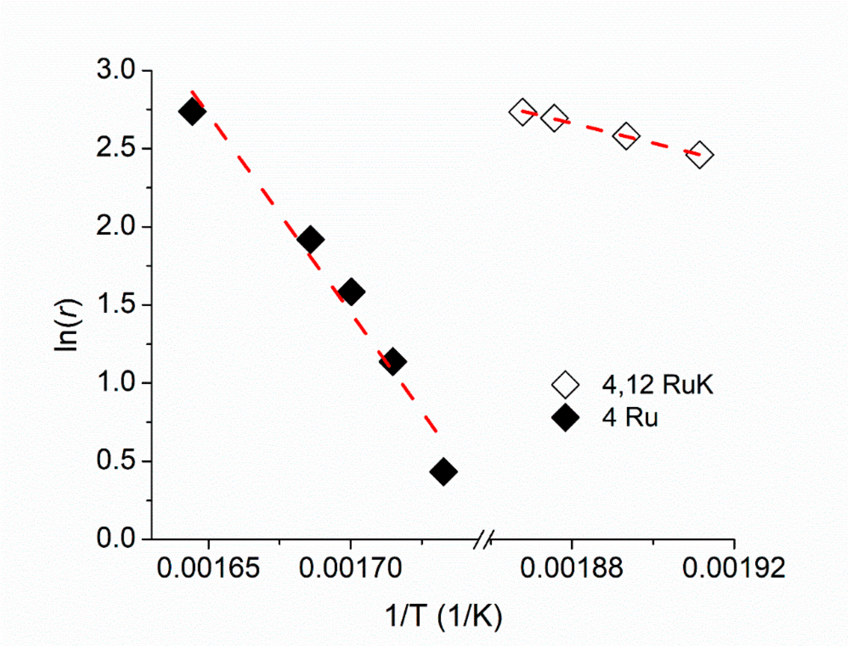

Figure S5. Arrhenius plot for 4 Ru (filled diamonds) and 4,12 RuK (open diamonds). Reaction conditions: 100% NH_3, 5,400 mL/hr/g_{cat}, and 1 bar. Measurements conducted under differential conditions.

Internal Mass Transfer Resistance

The Weis–Prater criterion was used to determine the absence of internal diffusion resistances. The Weis–Prater criterion is given by:

$$\frac{r_A' \rho_c R_P^2}{D_e C_{AS}} \ll 1$$

where r_A'= measured NH_3 reaction rate (mol/kg/s), ρ_c= catalyst pellet density (750 kg/m^3), R_P^2= pellet radius (2.25x10^{-5} m), D_e=effective diffusivity of NH_3 in the catalyst pellet, and C_{AS}= NH_3 concentration at the pellet surface (16.7 mol/m^3). Effective diffusivity is calculated by:

$$D_e = \frac{D_{NH3-H2} \phi_p \sigma}{\tau}$$

where ϕ_p= pellet porosity, σ is the constriction factor, and τ is the tortuosity. Typical values for a catalyst pellet are ϕ_p=0.4, σ=0.8, and τ= 3 (values adapted from ref. 65). D_{NH3-H2} is the diffusion coefficient of NH_3 in H_2 at 400^{o}C and it is given by:

$$D_{NH3-H2} = \frac{0.00266T^{3/2}}{PM_{NH3-H2}^{1/2}\sigma_{NH3-H2}^{2}\Omega_D}$$

where T is the temperature (K), P is the pressure (bar), $M_{NH3-H2}=2*[(1/M_{NH3})+(1/M_{H2})]^{-1}$, M_{NH3}=molecular weight of NH_3, M_{H2} = molecular weight of H_2, σ_{NH3-H2} = characteristic length (Å), and Ω_D is the diffusion collision integral (dimensionless) (adapted from ref. 74). D_e was found to be 3.51 $\times 10^{-4}$ m^2/s.

The measured reaction rate at 400°C for the unpromoted 4 Ru catalyst is 2.07 mol/kg/s. The LHS of the Weis–Prater criterion equates to 1.34×10^{-3}, which is much less than 1. Therefore, the criterion is satisfied.

XRD Analysis

Refer to main text for references for patterns of RuO_2, $KRuO_4$, KCl, and KRu_4O_8. Fig. S6–S32 show the XRD patterns for each catalyst. The CIF file no. is given for other species that are indexed in a pattern. . Table S1 is given to summarize the Ru species present in each catalyst, and additional speciation can be found with each XRD pattern. In instances where there are no entries in the table for a certain metal, there were no detectable Ru species present in the XRD patterns.

Table S1. Summary of the Ru species present in each catalyst

Ru, Secondary Metal,K Weight Loading	Secondary Metal	RuO_2	$KRuO_4$	KRu_4O_8
3,1,12	**Mg**	Y		Y
2,2,12		Y		
1,3,12		Y		
3,1,12	**Ca**			
2,2,12				
1,3,12			Y	
3,1,12	**Sr**		Y	
2,2,12			Y	
1,3,12				
3,1,12	**Sc**	Y	Y	
2,2,12		Y		
1,3,12		Y		
3,1,12	**Y**		Y	
2,2,12			Y	
1,3,12			Y	
3,1,12	**Zr**	Y		
2,2,12		Y	Y	
1,3,12		Y	Y	
3,1,12	**Hf**			
2,2,12			Y	
1,3,12			Y	
3,1,12	**Nb**	Y		
2,2,12		Y		
1,3,12		Y		
3,1,12	**Cr**	Y		Y
2,2,12		Y		
1,3,12				
3,1,12	**Mo**	Y	Y	
2,2,12		Y		
1,3,12		Y		
3,1,12	**W**	Y		
2,2,12		Y		
1,3,12		Y		

3,1,12				Y
2,2,12	**Mn**			Y
1,3,12				Y
3,1,12				
2,2,12	**Re**	Y		
1,3,12		Y		
3,1,12				Y
2,2,12	**Fe**			Y
1,3,12				
3,1,12				Y
2,2,12	**Os**			Y
1,3,12				
3,1,12				Y
2,2,12	**Co**	Y		
1,3,12				
3,1,12				Y
2,2,12	**Ir**		Y	Y
1,3,12			Y	Y
3,1,12		Y		
2,2,12	**Ni**	Y		
1,3,12				
3,1,12		Y		Y
2,2,12	**Pd**	Y		Y
1,3,12		Y		Y
3,1,12		Y		
2,2,12	**Pt**	Y		
1,3,12		Y		
3,1,12		Y		
2,2,12	**Cu**	Y		
1,3,12				
3,1,12				
2,2,12	**Ag**			
1,3,12				
3,1,12		Y		
2,2,12	**Au**	Y		
1,3,12		Y		
3,1,12			Y	
2,2,12	**Zn**	Y		
1,3,12		Y		
3,1,12			Y	
2,2,12	**Cd**		Y	
1,3,12			Y	
3,1,12		Y		
2,2,12	**In**	Y		
1,3,12		Y		
3,1,12	**Sn**			

2,2,12		Y		
1,3,12				
3,1,12	**Pb**			
2,2,12				
1,3,12				
3,1,12	**Bi**			
2,2,12				
1,3,12				

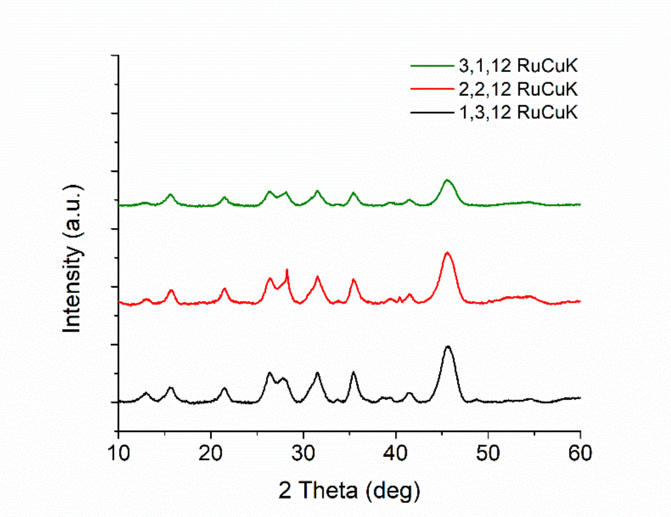

Figure S6. XRD patterns of (from bottom to top): 1,3,12 RuCuK, 2,2,12 RuCuK, and 3,1,12 RuCuK

Phase	cif no.	Present in:		
		3,1,12	2,2,12	1,3,12
RuO_2		Y	Y	
KRu_4O_8				
$KRuO_4$				
KCl				
$KCuO_2$	96-153-0994	Y	Y	Y
$KClO_2$	96-201-4619	Y	Y	Y

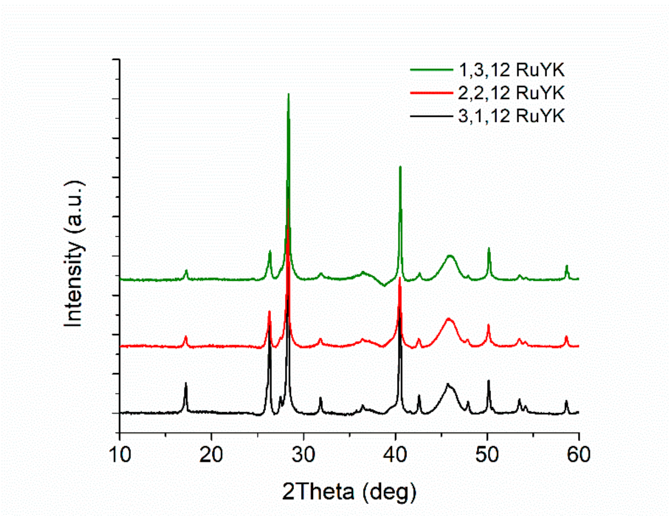

Figure S7. XRD patterns of (from bottom to top): 1,3,12 RuYK, 2,2,12 RuYK, and 3,1,12 RuYK

Phase	cif no.	Present in:		
		3,1,12	2,2,12	1,3,12

RuO_2				
KRu_4O_8				
$KRuO_4$		Y	Y	Y
KCl		Y	Y	Y

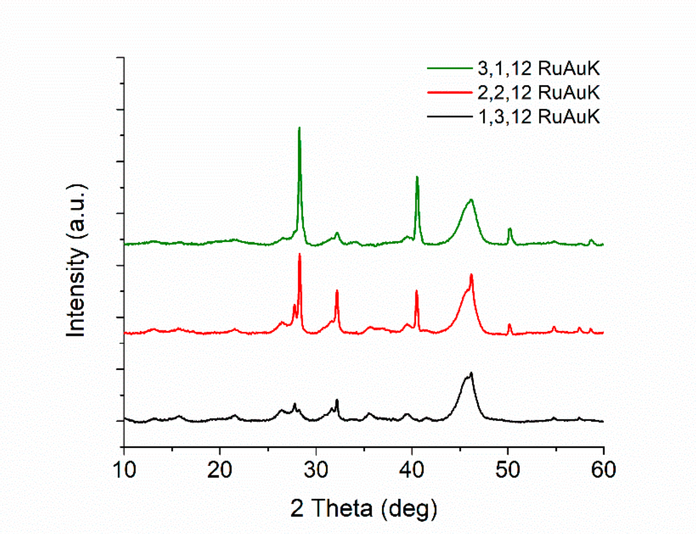

Figure S8. XRD patterns of (from bottom to top): 1,3,12 RuAuK, 2,2,12 RuAuK, and 3,1,12 RuAuK

Phase	cif no.	Present in:		
		3,1,12	2,2,12	1,3,12
RuO_2		Y	Y	Y
KRu_4O_8				
$KRuO_4$				
KCl		Y	Y	Y
Au	96-900-8464	Y	Y	Y

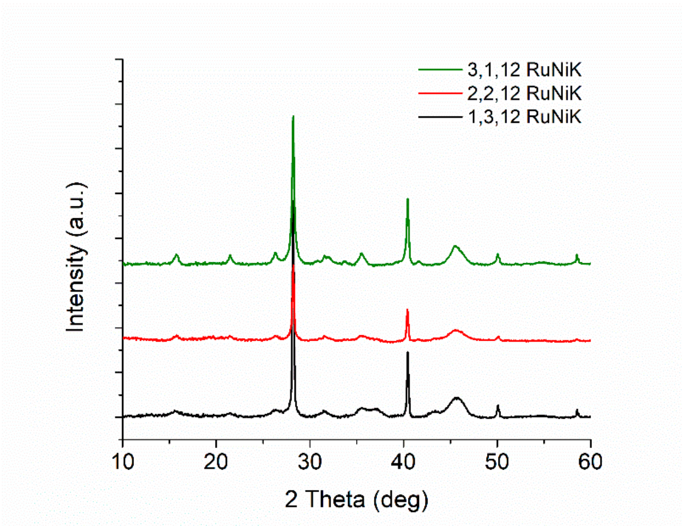

Figure S9. XRD patterns of (from bottom to top): 1,3,12 RuNiK, 2,2,12 RuNiK, and 3,1,12 RuNiK

Phase	cif no.	Present in:		
		3,1,12	2,2,12	1,3,12
RuO_2		Y	Y	
KRu_4O_8				
$KRuO_4$				
KCl		Y	Y	Y

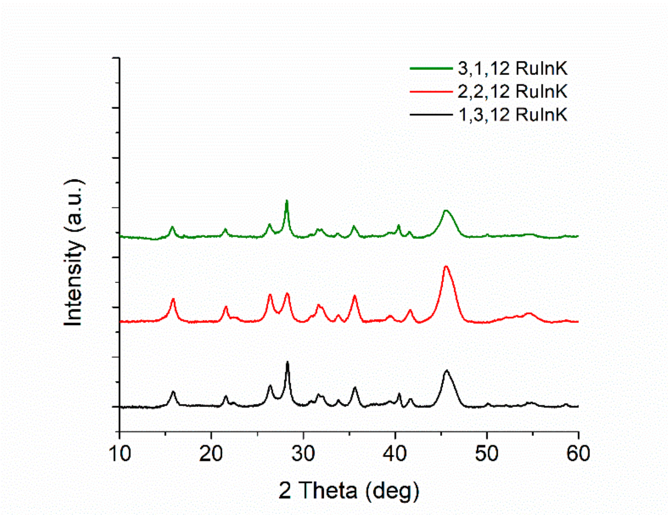

Figure S10. XRD patterns of (from bottom to top): 1,3,12 RuInK, 2,2,12 RuInK, and 3,1,12 RuInK

Phase	cif no.	Present in:		
		3,1,12	2,2,12	1,3,12
RuO_2		Y	Y	Y
KRu_4O_8				
$KRuO_4$				
KCl		Y		Y
In_2O_3	96-900-3113		Y	Y

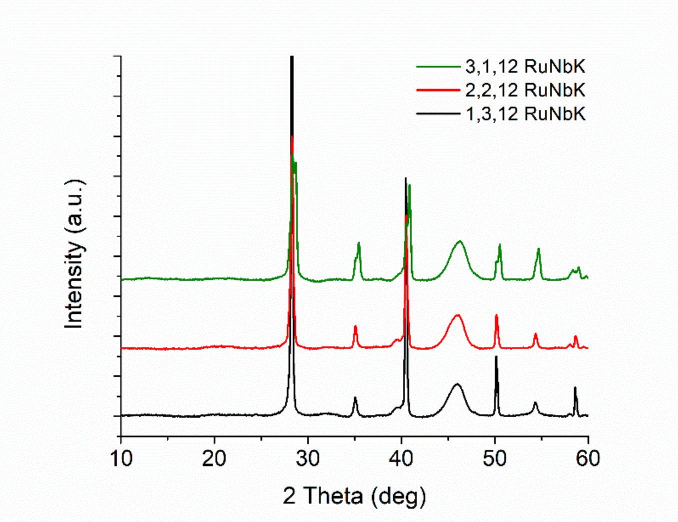

Figure S11. XRD patterns of (from bottom to top): 1,3,12 RuNbK, 2,2,12 RuNbK, and 3,1,12 RuNbK

Phase	cif no.	Present in:		
		3,1,12	2,2,12	1,3,12
RuO_2		Y	Y	Y
KRu_4O_8				
$KRuO_4$				
KCl		Y	Y	Y

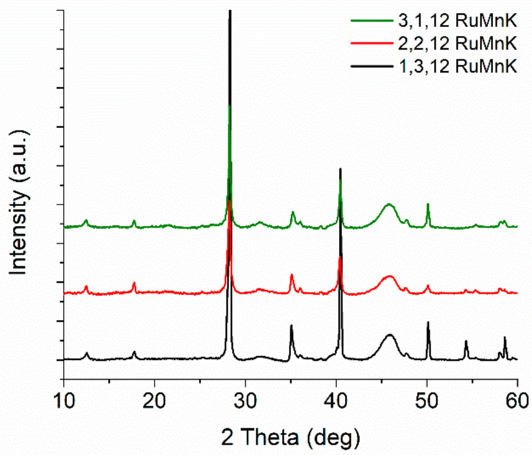

Figure S12. XRD patterns of (from bottom to top): 1,3,12 RuMnK, 2,2,12 RuMnK, and 3,1,12 RuMnK

Phase	cif no.	Present in:		
		3,1,12	2,2,12	1,3,12
RuO_2				
KRu_4O_8		Y	Y	Y
$KRuO_4$				
KCl		Y	Y	Y

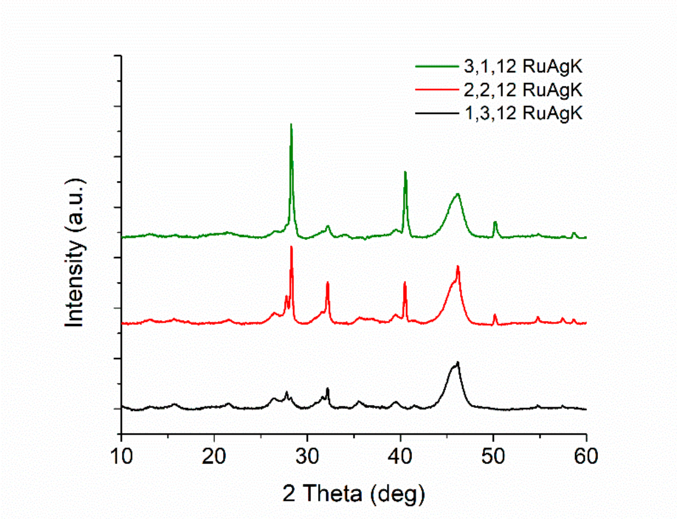

Figure S13. XRD patterns of (from bottom to top): 1,3,12 RuAgK, 2,2,12 RuAgK, and 3,1,12 RuAgK

Phase	cif no.	Present in:		
		3,1,12	2,2,12	1,3,12
RuO_2				
KRu_4O_8				
$KRuO_4$				
KCl		Y	Y	Y
AgCl	96-901-1667	Y	Y	Y

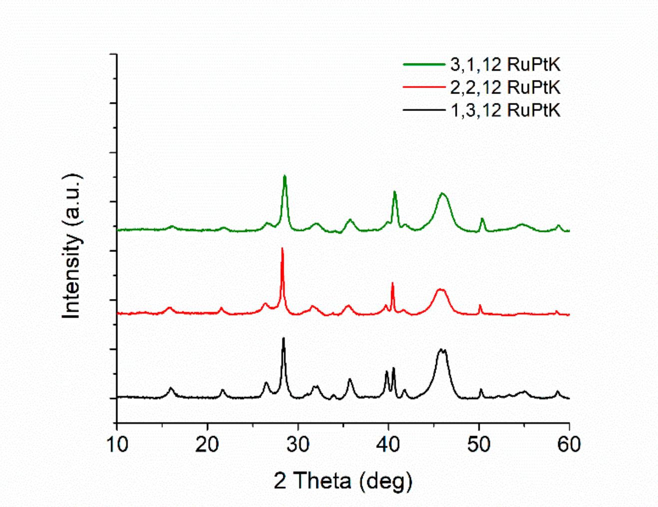

Figure S14. XRD patterns of (from bottom to top): 1,3,12 RuPtK, 2,2,12 RuPtK, and 3,1,12 RuPtK

Phase	cif no.	Present in:		
		3,1,12	2,2,12	1,3,12
RuO_2		Y	Y	y
KRu_4O_8				
$KRuO_4$				
KCl		Y	Y	Y
Pt	96-900-8481	Y	Y	Y

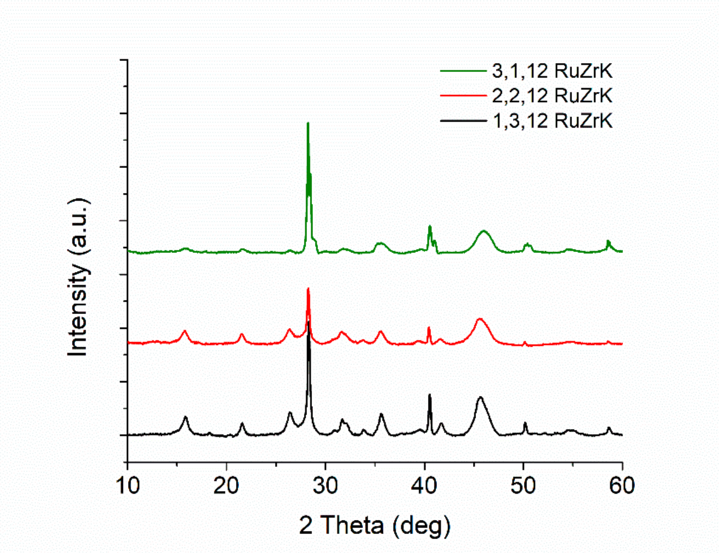

Figure S15. XRD patterns of (from bottom to top): 1,3,12 RuZrK, 2,2,12 RuZrK, and 3,1,12 RuZrK

Phase	cif no.	Present in:		
		3,1,12	2,2,12	1,3,12
RuO_2		Y	Y	Y
KRu_4O_8				
$KRuO_4$			Y	Y
KCl		Y	Y	Y
ZrO_2	96-900-5834	Y	Y	Y

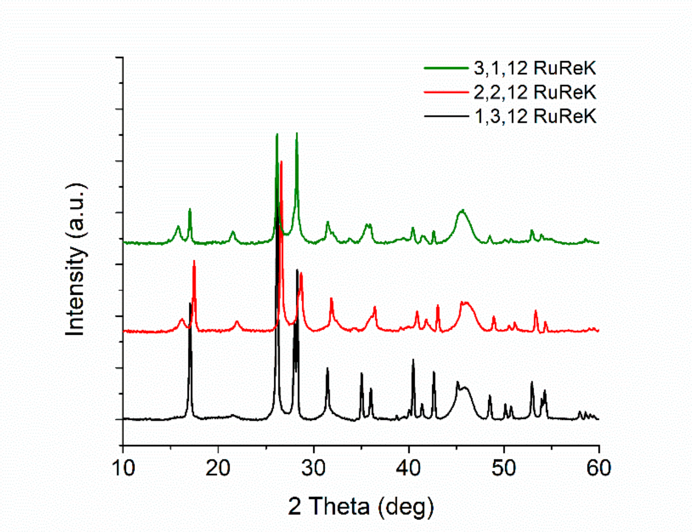

Figure S16. XRD patterns of (from bottom to top): 1,3,12 RuReK, 2,2,12 RuReK, and 3,1,12 RuReK

Phase	cif no.	Present in:		
		3,1,12	2,2,12	1,3,12
RuO_2			Y	Y
KRu_4O_8				
$KRuO_4$				
KCl		Y	Y	Y
$KReO_4$	96-200-1935	Y	Y	Y

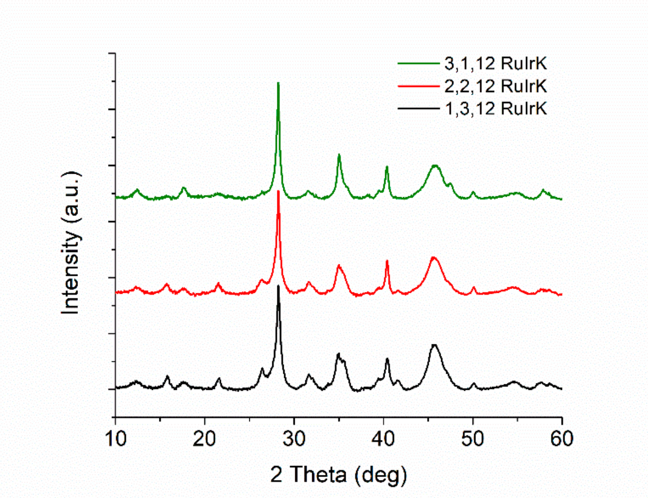

Figure S17. XRD patterns of (from bottom to top): 1,3,12 RuIrK, 2,2,12 RuIrK, and 3,1,12 RuIrK

Phase	cif no.	Present in:		
		3,1,12	2,2,12	1,3,12
RuO_2				
KRu_4O_8		Y	Y	Y
$KRuO_4$			Y	Y
KCl		Y	Y	Y
KIr_4O_8	96-433-8123	Y	Y	Y

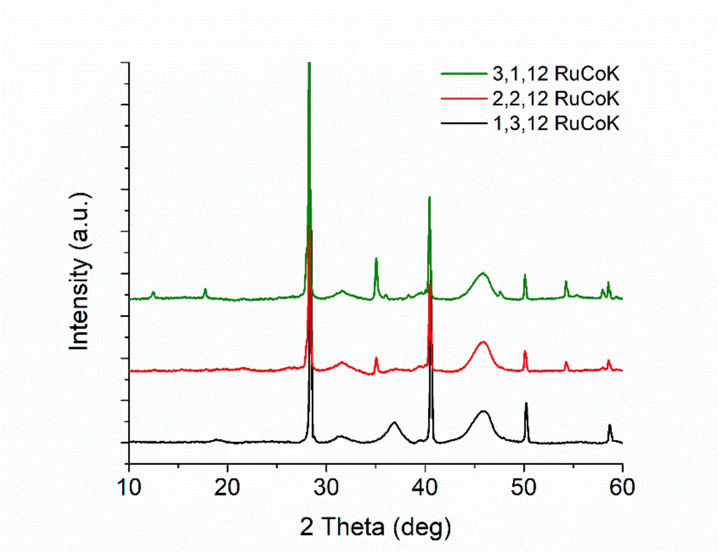

Figure S18. XRD patterns of (from bottom to top): 1,3,12 RuCoK, 2,2,12 RuCoK, and 3,1,12 RuCoK

Phase	cif no.	Present in:		
		3,1,12	2,2,12	1,3,12
RuO_2			Y	
KRu_4O_8		Y		
$KRuO_4$				
KCl		Y	Y	Y
Co_3O_4	96-153-4892		Y	Y

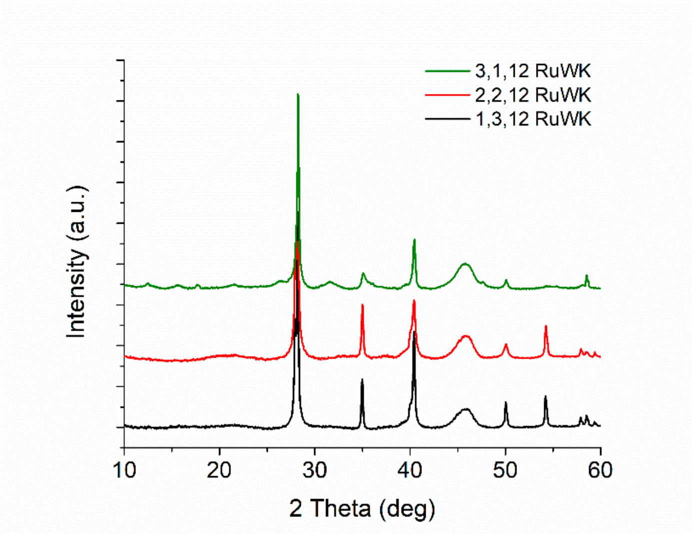

Figure S19. XRD patterns of (from bottom to top): 1,3,12 RuWK, 2,2,12 RuWK, and 3,1,12 RuWK

Phase	cif no.	Present in:		
		3,1,12	2,2,12	1,3,12
RuO_2		Y	Y	Y
KRu_4O_8				
$KRuO_4$				
KCl		Y	Y	Y

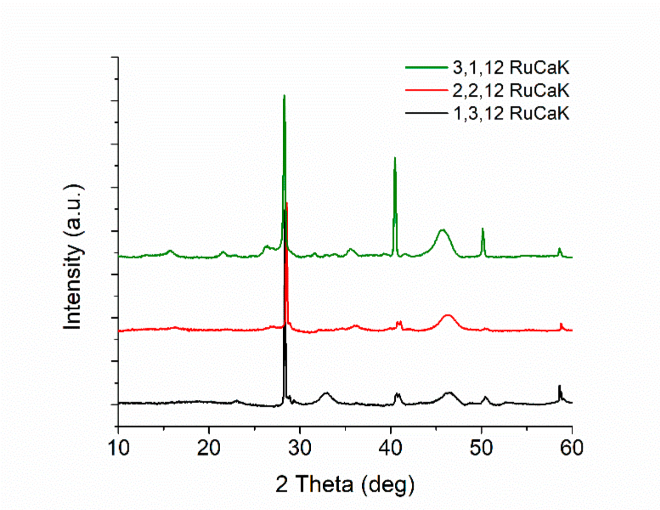

Figure S20. XRD patterns of (from bottom to top): 1,3,12 RuCaK, 2,2,12 RuCaK, and 3,1,12 RuCaK

Phase	cif no.	Present in:		
		3,1,12	2,2,12	1,3,12
RuO_2				
KRu_4O_8				
$KRuO_4$		Y		
KCl		Y	Y	Y

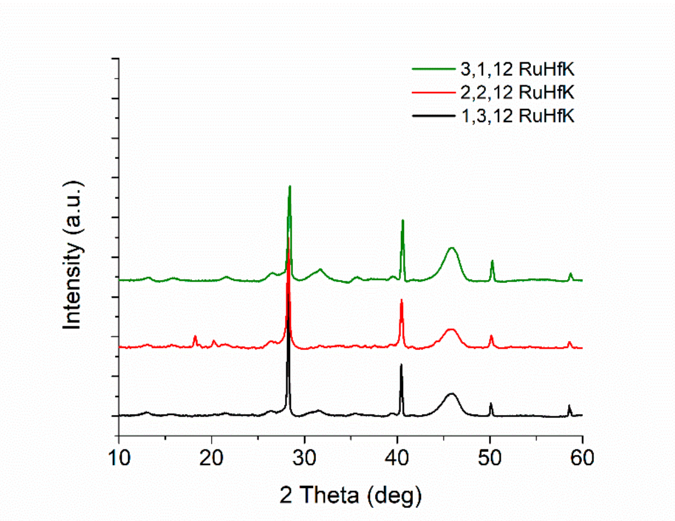

Figure S21. XRD patterns of (from bottom to top): 1,3,12 RuHfK, 2,2,12 RuHfK, and 3,1,12 RuHfK

Phase	cif no.	Present in:		
		3,1,12	2,2,12	1,3,12
RuO_2				
KRu_4O_8				
$KRuO_4$		Y	Y	
KCl		Y	Y	Y

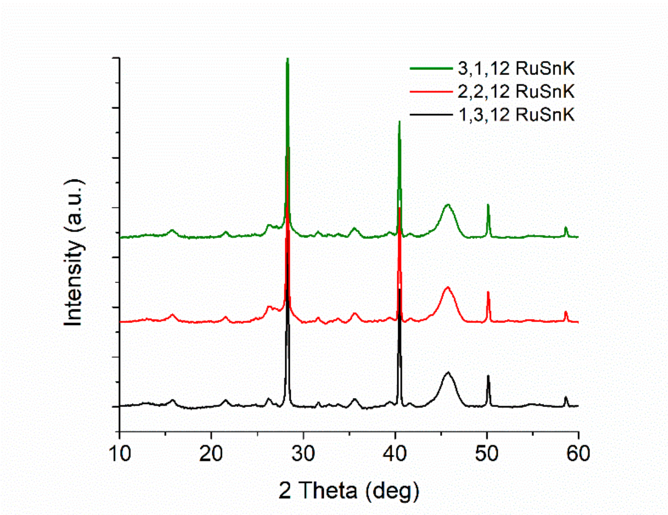

Figure S22. XRD patterns of (from bottom to top): 1,3,12 RuSnK, 2,2,12 RuSnK, and 3,1,12 RuSnK

Phase	cif no.	Present in:		
		3,1,12	2,2,12	1,3,12
RuO_2			Y	
KRu_4O_8				
$KRuO_4$				
KCl		Y	Y	Y

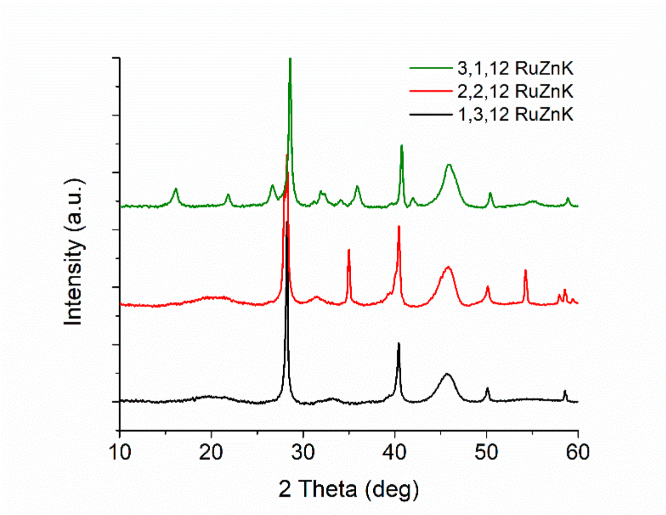

Figure S23. XRD patterns of (from bottom to top): 1,3,12 RuZnK, 2,2,12 RuZnK, and 3,1,12 RuZnK

Phase	cif no.	Present in:		
		3,1,12	2,2,12	1,3,12
RuO_2			Y	Y
KRu_4O_8				
$KRuO_4$		Y		
KCl		Y	Y	Y

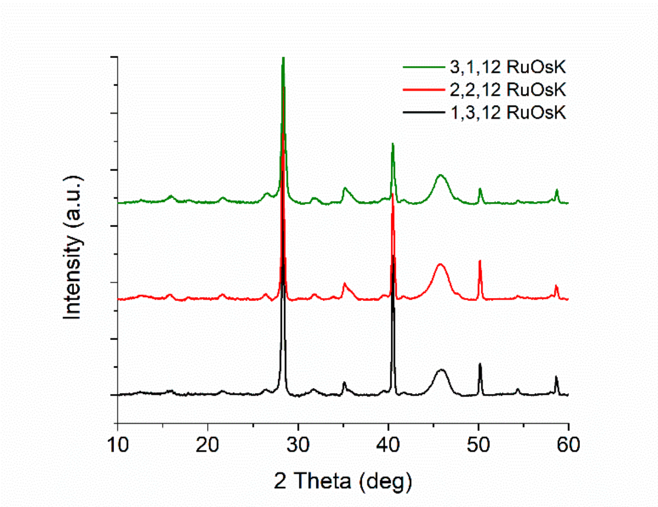

Figure S24. XRD patterns of (from bottom to top): 1,3,12 RuOsK, 2,2,12 RuOsK, and 3,1,12 RuOsK

Phase	cif no.	Present in:		
		3,1,12	2,2,12	1,3,12
RuO_2				
KRu_4O_8		Y	Y	
$KRuO_4$				
KCl		Y	Y	Y

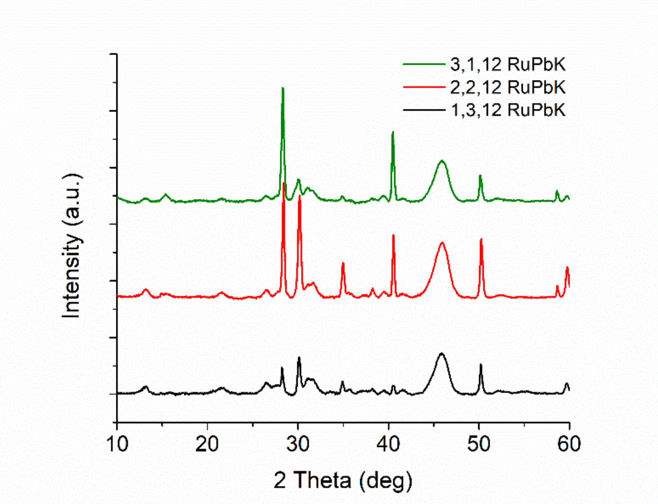

Figure S25. XRD patterns of (from bottom to top): 1,3,12 RuPbK, 2,2,12 RuPbK, and 3,1,12 RuPbK

Phase	cif no.	Present in:		
		3,1,12	2,2,12	1,3,12
RuO_2				
KRu_4O_8				
$KRuO_4$				
KCl		Y	Y	Y
PbO_2	96-900-8652	Y	Y	Y
Pb_3O_4	96-901-2125		Y	Y

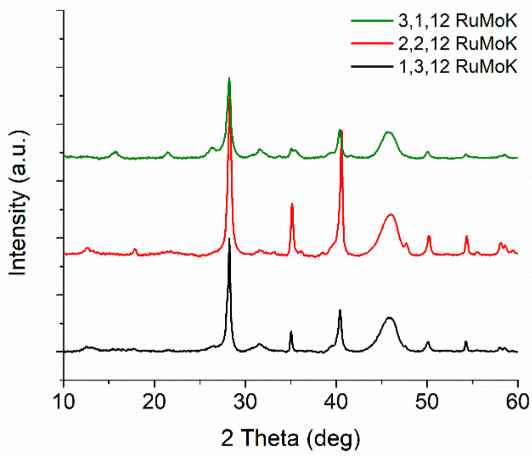

Figure S26. XRD patterns of (from bottom to top): 1,3,12 RuMoK, 2,2,12 RuMoK, and 3,1,12 RuMoK

Phase	cif no.	Present in:		
		3,1,12	2,2,12	1,3,12
RuO_2		Y	Y	Y
KRu_4O_8				
$KRuO_4$		Y		
KCl		Y	Y	Y

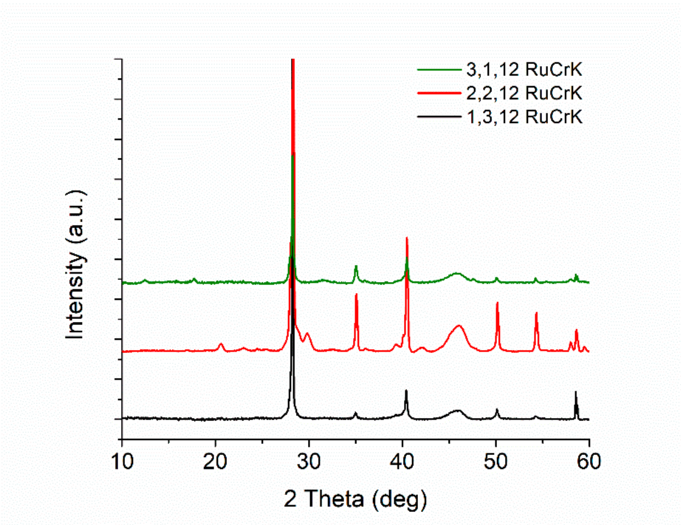

Figure S27. XRD patterns of (from bottom to top): 1,3,12 RuCrK, 2,2,12 RuCrK, and 3,1,12 RuCrK

Phase	cif no.	Present in:		
		3,1,12	2,2,12	1,3,12
RuO_2		Y	Y	
KRu_4O_8		Y		
$KRuO_4$				
KCl		Y	Y	Y
K_2CrO_4	96-900-7571		Y	

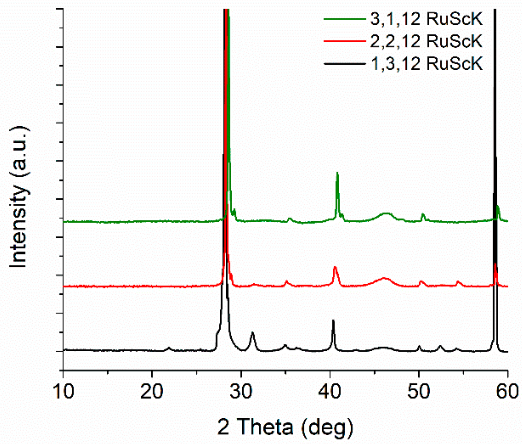

Figure S28. XRD patterns of (from bottom to top): 1,3,12 RuScK, 2,2,12 RuScK, and 3,1,12 RuScK

Phase	cif no.	Present in:		
		3,1,12	2,2,12	1,3,12
RuO_2		Y	Y	Y
KRu_4O_8		Y		
$KRuO_4$				
KCl		Y	Y	Y

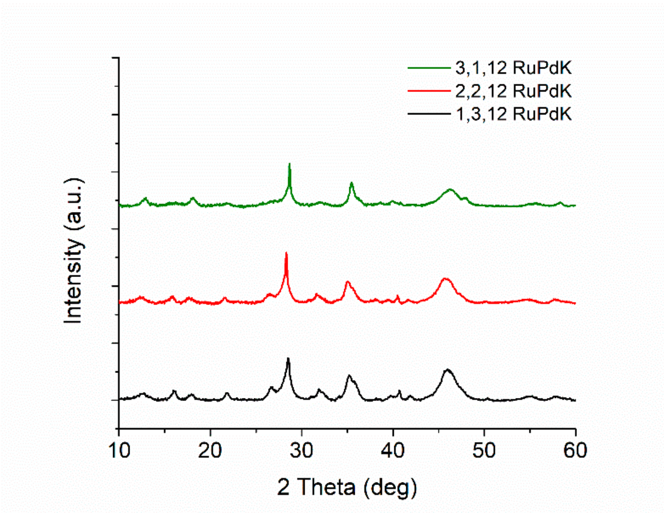

Figure S29. XRD patterns of (from bottom to top): 1,3,12 RuPdK, 2,2,12 RuPdK, and 3,1,12 RuPdK

Phase	cif no.	Present in:		
		3,1,12	2,2,12	1,3,12
RuO_2		Y	Y	Y
KRu_4O_8		Y	Y	Y
$KRuO_4$				
KCl			Y	Y
K_2PdCl_4	96-101-0316	Y	Y	Y

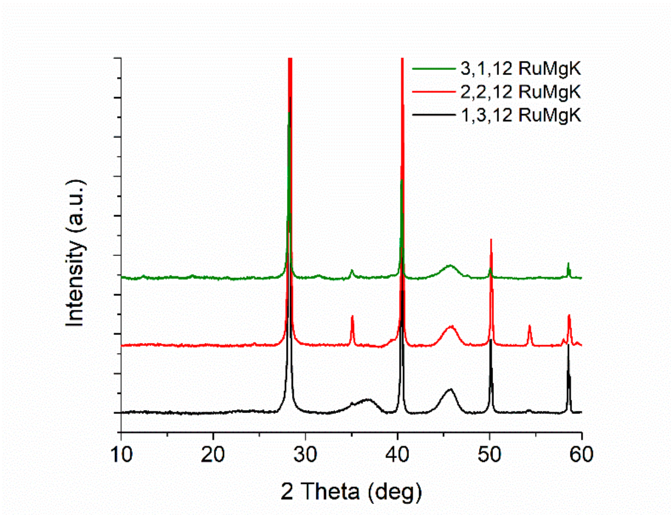

Figure S30. XRD patterns of (from bottom to top): 1,3,12 RuMgK, 2,2,12 RuMgK, and 3,1,12 RuMgK

Phase	cif no.	Present in:		
		3,1,12	2,2,12	1,3,12
RuO_2		Y	Y	Y
KRu_4O_8		Y		
$KRuO_4$				
KCl		Y	Y	Y

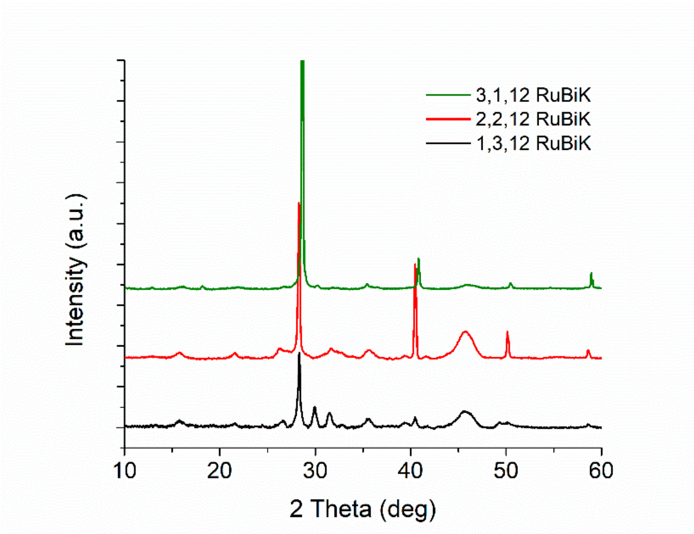

Figure S31. XRD patterns of (from bottom to top): 1,3,12 RuBiK, 2,2,12 RuBiK, and 3,1,12 RuBiK

Phase	cif no.	Present in:		
		3,1,12	2,2,12	1,3,12
RuO_2				
KRu_4O_8				
$KRuO_4$				
KCl		Y	Y	Y
Bi_2O_3	96-901-2328			Y

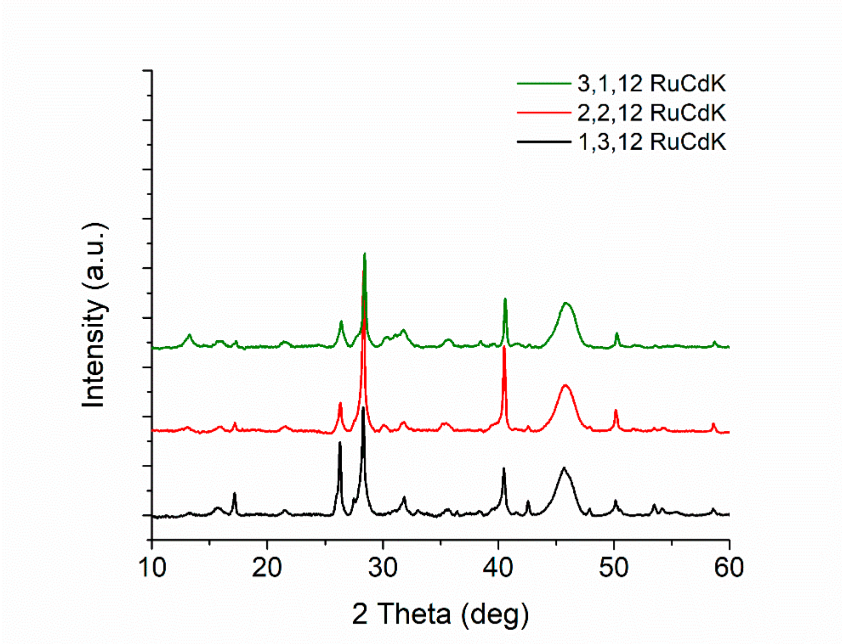

Figure S32. XRD patterns of (from bottom to top): 1,3,12 RuCdK, 2,2,12 RuCdK, and 3,1,12 RuCdK

Phase	cif no.	Present in:		
		3,1,12	2,2,12	1,3,12
RuO_2				
KRu_4O_8				
$KRuO_4$		Y	Y	Y
KCl		Y	Y	Y
CdO	96-900-6686			Y

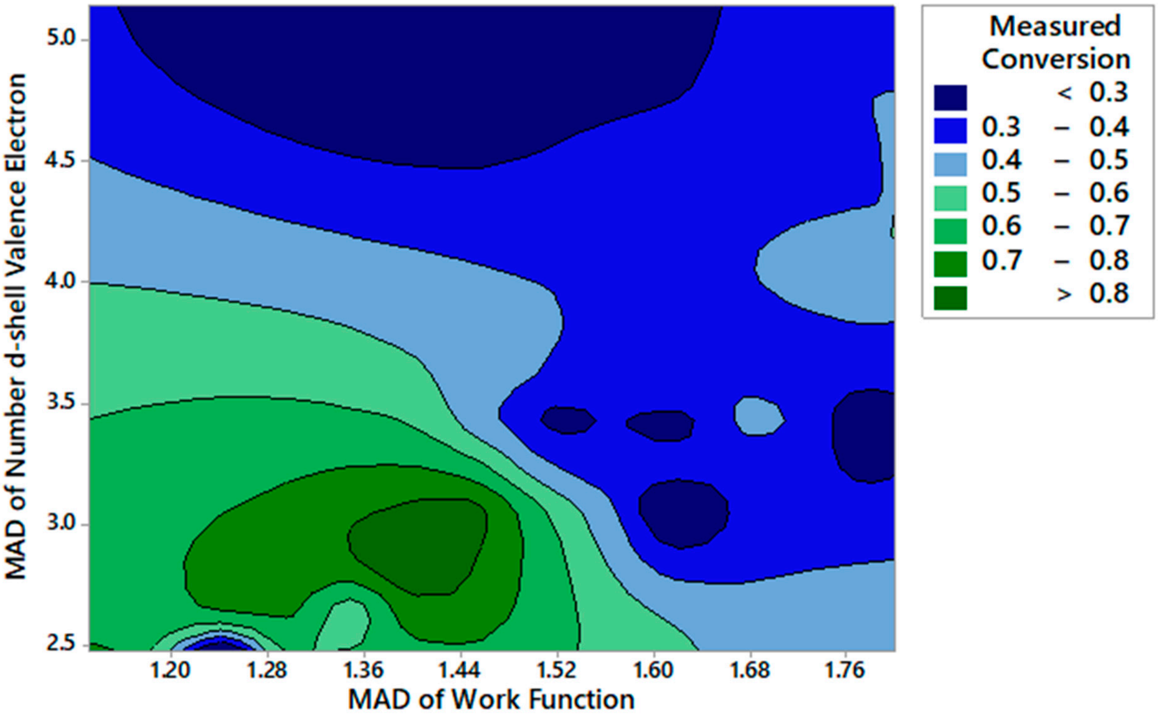

Figure S33. Ammonia decomposition activity at 300°C as a function of the mean absolute deviation (MAD) of the number of d-shell valence electrons and the MAD of the catalyst work function.